Preprints of the 21st IFAC World Congress (Virtual)
Berlin, Germany, July 12-17, 2020

An Application of Model-based Predictive Control for Renewables-intensive Power Distribution Grids

Nouha Dkhili * **David Salas** ** **Julien Eynard** *,***
Stéphane Thil *,*** **Stéphane Grieu** *,***

* *PROMES-CNRS (UPR 8521), Rambla de la thermodynamique, Tecnosud, 66100 Perpignan, France (nouha.dkhili@promes.cnrs.fr)*
** *Instituto de Ciencias de la Ingeniería, Universidad de O'Higgins, Rancagua, Chile (david.salas@uoh.cl)*
*** *Université de Perpignan Via Domitia, 52 Avenue Paul Alduy, 66860 Perpignan, France (julien.eynard@univ-perp.fr, stephane.thil@univ-perp.fr, grieu@univ-perp.fr)*

Abstract: in recent years, growing penetration of renewable-energy-based distributed generation into power distribution grids has been compromising operational constraints. In this paper, a model-based predictive control (MPC) strategy is proposed for demand/supply balance and voltage regulation in a power distribution grid with prolific distributed generation using flexible assets (water tower and biogas plant). Then, the impact that errors of photovoltaic (PV) power generation and grid load forecasts have on its performance is examined. Results show that the proposed control scheme is efficient and resilient to forecasting errors.

Keywords: MPC, distributed generation, flexible asset management, power distribution grids.

1. INTRODUCTION

The mounting levels of renewable-energy-based distributed generation in power distribution grids, especially PV power generation, introduces new operational challenges for grid operators. The inherently intermittent nature of the solar resource due to its dependency on weather conditions (Haupt et al. (2016)), coupled with the resulting bidirectional flow in power distribution grids, hampers grid stability and service quality (ENEDIS (2018)). For better monitoring and control of power distribution grids, the smart grid paradigm is born and rests on these building blocks: the enhancement of grid observability, through an advanced metering infrastructure (Mohassel et al. (2014)) and multi-horizon forecasting of grid load (Swan and Ugursal (2009)) and distributed generation (Wan et al. (2015), Gbémou et al. (2019)), the flexibility of power generation and power consumption within the power distribution grid, and smart management techniques to balance between supply and demand and comply with operational constraints (Dkhili et al. (2020)). In a modern grid, several distributed generation and storage device technologies coexist. The flexibility given by these devices can be used for a better operation of the grid and a guarantee of its stability (Pesaran et al. (2017), Sugihara et al. (2013)). This is the premise of the control strategy developed in the context of project Smart Occitania, whose objective is to demonstrate the feasibility of the smart grid concept for low-voltage power distribution grids with prolific distributed generation in rural and suburban areas.

In this paper, an application of MPC (Prodan and Zio (2014), Bruni et al. (2015), Petrollese et al. (2016), Parisio et al. (2017)) strategy for low-voltage power distribution grids is proposed. For a review of MPC for renewable energy applications, the reader is referred to Sultana et al. (2017). In this paper, the discrete MPC strategy uses third-party-owned distributed generators and storage systems (biogas plant and water tower) to balance supply and demand and prevent cases of overvoltage and undervoltage across the grid, in accordance with the assets' operational constraints. The water tower's operation is subject to an ON/OFF controller, making the problem a mixed-integer non-linear programming (MINLP) one, which is still a challenging active research field in applied mathematics. While several techniques could be implemented and tested, a relaxation of the problem, whether at the modelling stage or the resolution stage, is always required (the interested reader is referred to Lee and Leyffer (2012) for a modern survey of MINLP). The contribution of this paper is two-fold. First, an alternate formulation of the problem is proposed to bypass the MINLP framework without relaxing the ON/OFF controller constraint of the water tower. The proposed formulation treats the problem as a classical smooth non-linear optimisation, a setting whose theory and algorithms are known to be robustly developed (Nocedal and Wright (2006)). Second, a study is carried out of the MPC scheme's resilience to forecasting errors, with respect to the MPC scheme's sliding window length. Due to the non-convex nature of the problem, all presented results are local.

The paper is organised as follows: in section 2, models of the power distribution grid and the flexible assets used in this approach are given. Section 3 introduces the proposed control scheme, the optimisation problem, and

the forecasting method. In section 4, the case study treated throughout the paper is detailed. In section 5, results given by the MPC scheme are presented and an analysis of its resilience to forecasting errors is carried out. Finally, section 6 concludes the paper.

2. POWER DISTRIBUTION GRID AND FLEXIBLE ASSETS

Let H be the forecast horizon such that $H = H_p \cdot T$, with $T = 10\,\text{min}$ the time step and H_p the integer number of timeslots within the forecast horizon. In the following, and for all time-dependant quantities, $t \in \{1, \dots, H_p\}$.

2.1 Power distribution grid scheme

The proposed approach deals with supply/demand balance in a low-voltage power distribution grid equipped with distributed generation and power storage systems. Throughout this study, the inductive and capacitive aspects of the grid components are neglected. The data used in this study shows that reactive power at the transformer level of a suburban residential neighbourhood remains under 5% of the apparent power, which validates this assumption. For a given branch $[qj]$, the voltage drop between nodes q and j is given by Ohm's law, $\forall q, j \in \{1, \dots, N\}$, with N the number of nodes in the power distribution grid:

$$U_q(t) - U_j(t) = z_{qj}(t) \cdot I_{qj}(t) \tag{1}$$

where z_{qj} is the line impedance between nodes q and j and I_{qj} is the current flowing between nodes q and j.

Under the assumption that reactive power is negligible, U_q is the voltage at node q and is proportional to the active power consumed or produced at that node (P_q):

$$P_q(t) = U_q(t) \cdot I_q(t) \tag{2}$$

where I_q is the current injected into/absorbed by node q.

Herein, we focus on voltage constraints, which stipulate that the nominal voltage value be 230 V for single-phase connections, and 400 V for 3-phase connections (ENEDIS (2018)). Voltage means in a power distribution grid over 10 minutes must at all times remain within $\pm\ \delta U$ of the nominal value, i.e.:

$$|U_q(t) - U_n| \leqslant \delta U \tag{3}$$

where U_n (in V) is the nominal single-phase voltage value for all grid nodes and δU is the acceptable margin of voltage variations with respect to the nominal value (in France, 5% for power sub-transmission grids and 10% for power distribution grids).

2.2 Biogas plant

Biogas plants are renewable-energy-based distributed generators, connected to low-voltage power distribution grids. A biogas plant is composed of a bioreactor producing methane-filled biogas, a storage unit, and a power generator. The biogas volume in the storage unit (V_b) is expressed in m^3 and described as:

$$V_b(t+1) = V_b(t) + \frac{T}{60}\Big(Q_{b,in}(t) - Q_{b,out}(t)\Big) \tag{4}$$

with:

$$Q_{b,out}(t) = \frac{P_b(t)}{\eta \text{LHV}} \tag{5}$$

where $Q_{b,in}$ and $Q_{b,out}$ (in $\text{m}^3\,\text{h}^{-1}$) are the flow rates of biogas production entering the storage unit and biogas consumption by the power generator, respectively, P_b (in W) is the plant's active power output, η is the generator's efficiency, and LHV (in $\text{kWh}\,\text{m}^{-3}$) is the lower heating value of the stored biogas.

At each time step, the plant's active power output is subject to the following constraint:

$$P_{b,min} \leqslant P_b(t) \leqslant P_{b,max} \tag{6}$$

where $P_{b,min}$ and $P_{b,max}$ are the minimal and maximal power generation of the biogas plant, respectively.

Regarding the biogas volume in the storage unit, it is subject, at each time step, to the following constraint:

$$V_{b,min} \leqslant V_b(t) \leqslant V_{b,max} \tag{7}$$

where $V_{b,min}$ and $V_{b,max}$ are the minimal and maximal biogas storage capacities of the biogas plant, respectively.

2.3 Water tower

Water towers provide pressurized potable water supply and emergency water storage for fire protection. They are connected to low-voltage power distribution grids. The volume in the storage tank (V_w) is expressed in m^3 and described as follows:

$$V_w(t+1) = V_w(t) + \frac{T}{60}\Big(Q_{w,in}(t) - Q_{w,out}(t)\Big) \tag{8}$$

with:

$$Q_{w,in}(t) = \frac{P_w(t)\eta_w}{\rho g h} \tag{9}$$

where $Q_{w,in}$ and $Q_{w,out}$ (in $\text{m}^3\,\text{h}^{-1}$) are the flow rates of water entering the storage tank and water consumption, respectively, P_w (in W) is the water pump's active power consumption, η_w is the water pump's efficiency, ρ (in $\text{kg}\,\text{m}^{-3}$) is the water density, g (in $\text{m}\,\text{s}^{-2}$) is the gravitational acceleration, and h (in m) is the water level in the storage tank.

Let $P_{w,min}$ and $P_{w,max}$ be the minimum and maximum power consumption values of the water tower, respectively. P_w can only be set following ON/OFF commands, i.e. it is subject to the following constraint:

$$P_w \in \{P_{w,min}; P_{w,max}\} \tag{10}$$

At each time step, the water volume in the storage tank is subject to the following constraint:

$$V_{w,min} \leqslant V_w(t) \leqslant V_{w,max} \tag{11}$$

where $V_{w,min}$ and $V_{w,max}$ are the minimal and maximal water storage capacities of the water tank, respectively.

3. SMART MANAGEMENT SCHEME

3.1 Optimisation problem

The optimisation problem at hand consists in reducing the gap between power generation and consumption in a power distribution grid. To do so, third-party-owned biogas plant and water tower are used to balance out the discrepancies in the grid's supply/demand equilibrium. $P_{cons} \in \mathbb{R}^{H_p}$ is the grid load (in W), and $P_{PV} \in \mathbb{R}^{H_p}$ is the PV power generation (in W). The control variables are

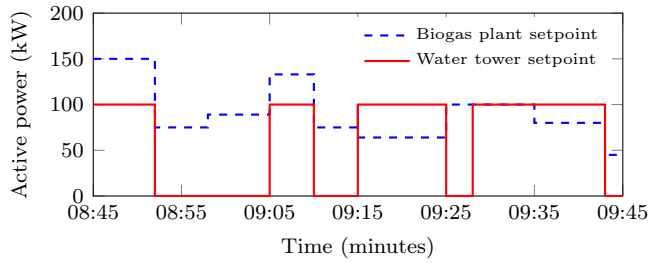

Fig. 1. Example of flexible assets' setpoints using the switch control model.

$P_b \in \mathbb{R}^{H_p}$ and $P_w \in \mathbb{R}^{H_p}$, which represent the active power setpoints for the biogas plant generation and the water tower consumption.

To outmanoeuvre the handicaps caused by the MINLP setting, an alternate formulation of the optimisation problem is proposed, which rests on the introduction of a new optimisation variable $\bar{t} \in \mathbb{R}^{H_p}$. Between time steps t_i and t_{i+1}, the water tower can switch between its two states of operation ($P_{w,min}$ and $P_{w,max}$), the instant at which this switch occurs is denoted $\bar{t}_i$. Simultaneously, the biogas plant setpoint may also switch from one value to another, although the biogas plant setpoint does not have to change between sampling times when that of the water tower does if it is unnecessary. Therefore, setpoints of biogas plant power generation and water tower power consumption are no longer constant during a given time step. Only one state switch is permitted within each time step.

Let us denote $X = [P_{b,\mathrm{ON}}\ P_{b,\mathrm{OFF}}\ \bar{t}\ U_{\mathrm{ON}}\ U_{\mathrm{OFF}}]^\mathsf{T}$, where $P_{b,\mathrm{ON}} \in \mathbb{R}^{H_p}$ and $P_{b,\mathrm{OFF}} \in \mathbb{R}^{H_p}$ form the biogas plant setpoint as follows, $\forall i \in \{1, \dots, H_p\}$:

$$P_b(t) = \begin{cases} P_{b,\mathrm{ON}}(i) & t \in [t_i, t_i + \bar{t}_i] \\ P_{b,\mathrm{OFF}}(i) & t \in [t_i + \bar{t}_i, t_{i+1}] \end{cases} \tag{12}$$

For every grid node $q \in \{1, \dots, N\}$, $U_{\mathrm{ON}} \in \mathbb{R}^{H_p \times N}$ and $U_{\mathrm{OFF}} \in \mathbb{R}^{H_p \times N}$ form the voltages in the grid as follows, $\forall i \in \{1, \dots, H_p\}$:

$$U_q(t) = \begin{cases} U_{\mathrm{ON}}(i,q) & t \in [t_i, t_i + \bar{t}_i] \\ U_{\mathrm{OFF}}(i,q) & t \in [t_i + \bar{t}_i, t_{i+1}] \end{cases} \tag{13}$$

Without loss of generality, the problem can be solved assuming that the first state of the water tower is always ON, and at times $\bar{t}$, it switches to OFF. Figure 1 gives an example of what the flexible assets' setpoints would look like using the switch control model. In fact, we can see that the transition between states doesn't only occur at the beginning of each time step. The proposed problem is then formulated as follows:

$$\begin{aligned} X^* = \arg\min_X \sum_{i=0}^{H_p-1} \\ \Bigg[\int_{t_i}^{t_i+\bar{t}_i} |P_{PV}(t) + P_b(t) - P_{cons}(t) - P_{w,max}|^2 dt \\ + \int_{t_i+\bar{t}_i}^{t_{i+1}} |P_{PV}(t) + P_b(t) - P_{cons}(t) - P_{w,min}|^2 dt \Bigg] \end{aligned} \tag{14}$$

subject to bounds and constraints formulated hereinafter, $\forall i \in \{1, \dots, H_p\}$.

- Biogas plant power bounds:

$$P_{b,min} \leqslant P_{b,\mathrm{ON}}(i) \leqslant P_{b,max} \tag{15}$$
$$P_{b,min} \leqslant P_{b,\mathrm{OFF}}(i) \leqslant P_{b,max} \tag{16}$$

- Switch time bounds:

$$0 \leqslant \bar{t}_i \leqslant T \tag{17}$$

- Biogas volume constraints:

$$V_{b,min} \leqslant V_b(t) \leqslant V_{b,max} \tag{18}$$

- Water volume constraints:

$$V_{w,min} \leqslant V_w(t) \leqslant V_{w,max} \tag{19}$$

- Voltage constraints:

$$\bar{t}_i \cdot K(P_{b,\mathrm{ON}}(i), P_{w,max}, U_{\mathrm{ON}}(i)) = 0 \tag{20}$$
$$(T - \bar{t}_i) \cdot K(P_{b,\mathrm{OFF}}(i), P_{w,min}, U_{\mathrm{OFF}}(i)) = 0 \tag{21}$$
$$|U_{\mathrm{ON}}(i) - U_n| \leqslant \delta U \tag{22}$$
$$|U_{\mathrm{OFF}}(i) - U_n| \leqslant \delta U \tag{23}$$

$K(P_b(t), P_w(t), v(t))$, with $v(t) = [U_1(t)\ U_2(t) \cdots U_N(t)]^\mathsf{T}$, represents the equation set derived from Kirchhoff's laws, describing voltage variations across the grid as a function of the powers injected/absorbed at each node. The voltage variation between nodes i and j follows Kirchhoff's law equations. Kirchhoff's law constraints are presented as two sets of constraints (20) and (21) which guarantee that Kirchhoff's laws are upheld in both sub-intervals of each time step. Equation set (20) sees the equation set depicting voltage variations multiplied by $\bar{t}_i$ whereas equation set (21) sees it multiplied by $(T - \bar{t}_i)$, using appropriate values of biogas plant and water tower setpoints for each interval, to ensure that only one constraint is activated in case of extreme values of $\bar{t}$. In fact, in case $\bar{t}_i = 0$, equation set (20) is eliminated. This reflects the fact that during time step i, the water tower is turned off immediately at the beginning of the time step. Similarly, in case $\bar{t}_i = T$, equation set (21) is eliminated since the water tower remains on for the duration of the time step. Voltage constraints are also written as two sets of constraints (22) and (23) that account for voltage variations in both states of the grid within each time step.

3.2 Forecast module

For a better regulation of the power distribution grid, variations of uncontrollable quantities which compromise its stability must be forecasted. In this study, these quantities are the grid load and PV power generation over the scheme's forecast horizon. At each time step, the MPC scheme integrates the updated forecasts into the optimisation problem.

In this study, both quantities are predicted using Gaussian process regression (GPR) (Rasmussen and Williams (2006)), a probabilistic non-parametric model completely defined by its mean function and covariance function. There exists previous works in the literature using GPR for PV power generation forecasting (Rohani et al. (2018), Gbémou et al. (2019)) as well as short-term grid load forecasting (Mori and Ohmi (2005)). Kernel compositions that take into account both the periodic component of the quantities at hand and the added fluctuations are

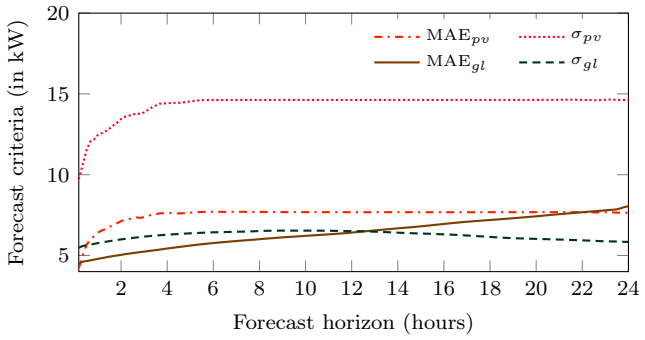

Fig. 2. Mean absolute error and standard deviation of PV power generation forecasts (MAE$_{pv}$, σ_{pv}) and grid load forecasts (MAE$_{gl}$, σ_{gl}) with respect to forecast horizons ranging from 10 minutes to 24 hours.

used. For an in depth study of the kernel study performed beforehand, the reader is referred to Tolba et al. (2019). The mean absolute error (MAE) and standard deviation (σ) of the forecasts for PV power generation and grid load are displayed in Fig. 2, for forecast horizons ranging from 10 minutes to 24 hours. For small forecast horizons, forecasting errors increase as the horizon's length does. However, it is interesting to note that forecasting errors for long horizons remain constant. This may seem counter-intuitive but is indeed due to the structure of the GPR model defined by the expression of its kernel (or herein, kernel composition). In cases where the developed GPR model is unable to provide reliable forecasts, as is the case here for long forecast horizons, it gives forecasts that resemble the basic shape of its kernel, hence the steady error values.

4. CASE STUDY

From the medium-voltage/low-voltage (MV/LV) transformer point of view, a power distribution grid can be seen as equivalent to the configuration given in Fig. 3, provided that the power lines' inductive and capacitive effects are neglected. Here, $U_n = 230$V and δU is set to be be 10% of U_n, that is $\delta U = 23$V. Since data used in this case study comes from a small suburban residential neighbourhood (approximately $1\,\mathrm{km}^2$), all line impedances are assumed identical, i.e. $z_{qj} = z$, $\forall q, j \in \{0, \ldots, 5\}$. The study presented herein is carried out in a simulated low-voltage power distribution grid, whose equivalent electrical circuit is shown in Fig. 3. It contains the following elements.

- End-consumer: grid load data are provided by CAHORS group, and correspond to transformer-level measurements of power consumption in a suburban neighbourhood in the south of France (Fig. 4).
- Water tower with the following characteristics: $V_{w,max} = 400\,\mathrm{m}^3$, $V_{w,min} = 0\,\mathrm{m}^3$, $P_{w,min} = 0\,\mathrm{kW}$, and $P_{max} = 100\,\mathrm{kW}$. The water pump's "default operation" is subject to an ON/OFF controller: when the water level in the tank reaches its minimum $V_{w,min}$, the pump is turned on at its nominal power ($P_{w,n} = 100\,\mathrm{kW}$) and continues to fill the tank until the water reaches the maximum level $V_{w,max}$.
- PV power generation: data used for the simulations correspond to PV power generation from 50 household PV panels based on global horizontal irradiance (GHI) data given by a sensor placed on the roof of the laboratory PROMES-CNRS (Fig. 4), a few kilometres away from the same suburban neighbourhood.
- Biogas plant with the following characteristics: $V_{b,max} = 400\,\mathrm{m}^3$, $V_{b,min} = 0\,\mathrm{m}^3$, $Q_{b,in} = 50\,\mathrm{m}^3\,\mathrm{h}^{-1}$, LHV $= 5\,\mathrm{kWh\,m}^{-3}$, $P_{b,n} = 100\,\mathrm{kW}$ (nominal power generation), $P_{b,min} = 0\,\mathrm{kW}$, $P_{b,max} = 200\,\mathrm{kW}$, and $\eta = 0.4$. The biogas plant's "default operation" sees a steady stream of biogas production entering the storage unit ($Q_{b,in}$), and constant power generation ($P_{b,n} = 100\,\mathrm{kW}$) injected into the power distribution grid.

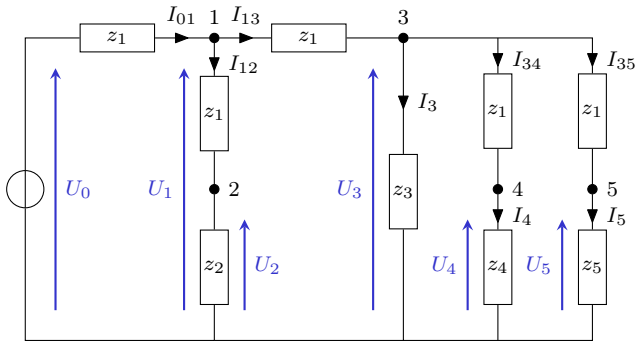

Fig. 3. Equivalent electrical circuit of the low-voltage power distribution grid. Let z_1, z_2, z_3, z_4, and z_5 be the line impedance, the impedances of the water tower's pump (node 2), the building (node 3), the biogas plant's generator (node 4), and the PV installation (node 5), respectively. U_1, U_2, U_3, U_4 and U_5 are voltages throughout the power distribution grid.

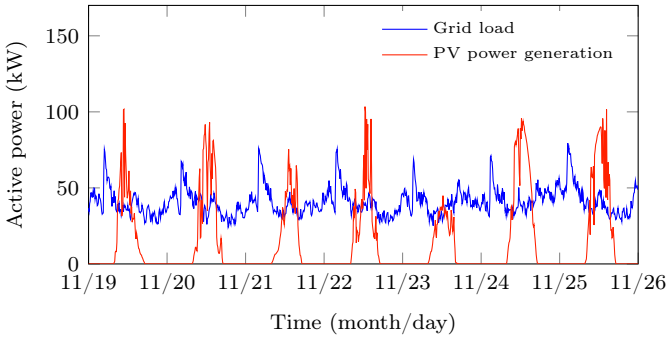

Fig. 4. Grid load and PV power generation data over a November week.

Grid load and PV power generation data used in the case study are presented in Fig. 4 hereinabove.

5. RESULTS AND ANALYSIS

In this section, simulation results are presented and analysed. Resolution of the optimisation problem is done through nonlinear interior point algorithm in MATLAB. The initial supply/demand gap before optimisation is an evaluation of the objective function using grid load and PV power generation data shown in Fig. 4 and flexible assets' "default operation" as explained in section 4. The reference strategy is a weekly planning assuming "perfect" forecasts, i.e. that uses data. This planning is based on an optimisation problem where the ON/OFF constraint of the water tower's operation is relaxed.

The performance of the MPC scheme using grid load and PV power generation forecasts, updated at each sampling time, is evaluated with respect to two criteria. The first is the length of its sliding window, and therefore the forecast horizon, and the second is results the scheme provides when, instead of forecasts, measured data are used throughout the simulation period.

The algorithm updates the forecasts injected into the optimisation problem at each time step. The final objective function values given by the algorithm at various sliding window sizes are shown in Fig. 5. The final objective value's lower bound is 1,360 kW, given by the reference strategy. The algorithm approaches this bound as the sliding window gets bigger since more information about the system's future behaviour and disturbances are incorporated. In both the scheme with "perfect" forecasts and the one with GPR forecasts, the final objective function value steadily decreases as the sliding window size gets bigger, with values for both schemes remaining close to one another and reaching their lowest at the 24-hour window for both schemes. For the former, the final objective function value goes from 1,764.4kW for a 1-hour window to 1,424.9kW for a 24-hour window. For the latter, the final objective function value goes from 1,788.4kWfor a 1-hour window to 1466.8kW for a 24-hour window.

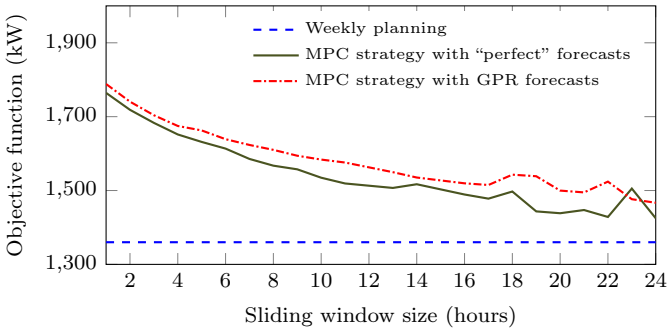

Fig. 5. The final objective function value per sliding window size. The initial supply/demand gap is 2,808 kW.

Although forecasting errors grow as the forecast horizon gets longer, the closed-loop structure of MPC protects it from substantial performance degradation as the sliding window size gets bigger. The difference in objective function values created by forecasting errors is at its lowest for a 23-hour window (-28.825kW) and at its highest for a 22-hour window (95.673kW). As is illustrated by Fig. 6, the mean number of function evaluations per window needed for the algorithm to converge to a solution when using GPR forecasts of grid load and PV power generation is consistently bigger than that needed when the forecasts are "perfect", which infers a longer running time. On average, the use of GPR forecasts adds 26.05% to the mean number of function evaluations per window. The additional computational burden is at its maximum for the 20-hour window, with an extra 47.83% of function evaluations with respect to the scheme that uses "perfect" forecasts.

Another pertinent aspect to study is the constraint violation caused by forecasting errors. In all the simulations studied herein, biogas volume and water volume constraints are upheld. But, the algorithm is not always

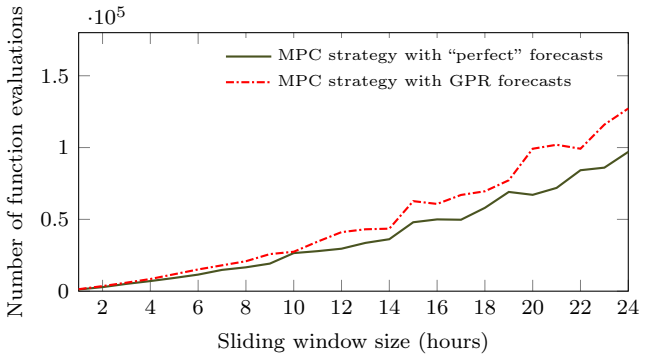

Fig. 6. The mean number of function evaluations the algorithm needs to converge to a solution for each sliding window size.

able to perfectly satisfy voltage constraints, namely the Kirchhoff's laws equation set depicting voltage variations throughout the power distribution grid. This stems from the fact that real PV power generation and grid load values, over the following 10 minutes during which the first setpoint is executed, are slightly different from the forecasted ones. Therefore, the real values might not satisfy Kirchhoff's laws even though the forecasted ones do. These discrepancies result in violations of the voltage equality constraints. The maximum voltage constraint violation is much higher when using GPR forecasts, as evidenced by Fig. 7. As a matter of fact, the maximum constraint violation when using "perfect" forecasts do not exceed 0.01V. When using GPR forecasts, however, the maximum voltage constraint violation averages at 0.10V, reaching its highest value at hour 22 (0.40V).

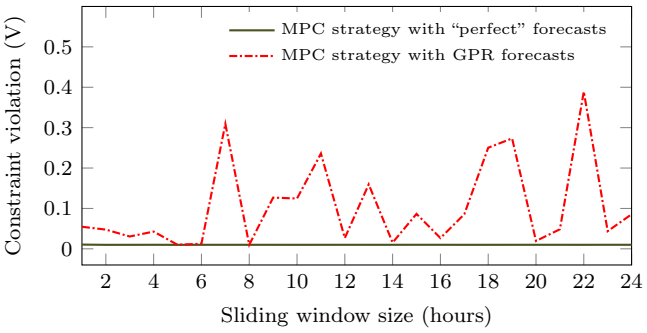

Fig. 7. Maximum voltage constraint violation per sliding window size.

In a nutshell, results show that forecasting errors for PV power generation and grid load cause an additional computational burden to the control algorithm, which already needs an increasing number of function evaluations in order to reach a feasible solution as the sliding window gets larger. In addition, these errors create instances of voltage constraint violation which are higher than the weekly planning, but remain small in amplitude. A slight degradation of the final objective function value as a result of forecasting errors is also observed. However, the control scheme still proves itself resilient by improving its final objective function value as the sliding window gets larger, and this value remains within reasonable margin of the one given by the scheme when using "perfect" forecasts.

The choice of the sliding window size for the MPC scheme is a compromise between the final objective function value and the computational burden. In this study, a 14-hour window is chosen. The temporal evolution of the biogas plant's power generation setpoints and the water tower's power consumption setpoints given by the various schemes for this window size are tracked in Fig. 8 and Fig. 9. The setpoints given by the MPC scheme show a clear departure from both the initial setpoints and the ones given by the weekly planning. Particularly in the case of the biogas plant setpoint, a periodic behaviour emerges. The temporal evolution of the gap between supply and demand given by the various schemes using a 14-hour window are presented in Fig. 10. For both MPC schemes (with "perfect" or GPR forecasts), considerable reduction of this gap is observed. Both schemes have similar behaviour, as their values of supply/demand gap fluctuate around the constant and minimal level achieved by the weekly planning. These results show that, even though the supply/demand gap obtained when the MPC scheme uses GPR forecasts remains close to the one obtained when it uses data, the setpoint in the case of GPR forecasts are afflicted with significant fluctuations which diminish their implementability.

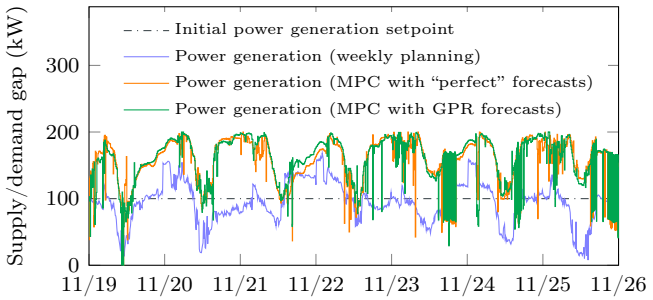

Fig. 8. Power generation setpoints given by the MPC strategy with "perfect" or GPR forecasts using a 14-hour sliding window, with respect to the initial gap and the one given by the weekly planning.

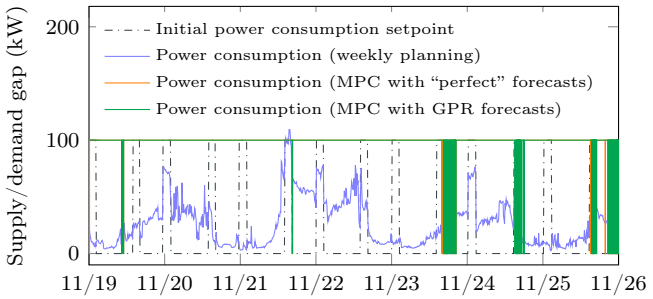

Fig. 9. Power consumption setpoints given by the MPC strategy with "perfect" or GPR forecasts using a 14-hour sliding window, with respect to the initial gap and the one given by the weekly planning.

6. CONCLUSION

In this paper, an MPC scheme for the smart management of third-party-owned flexible assets in a low-voltage power distribution grid with high penetration of PV power generation is proposed.

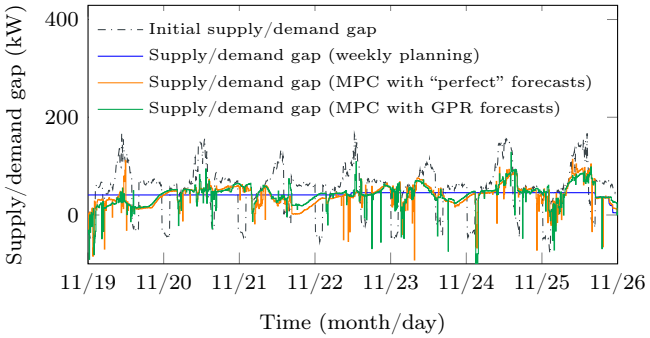

Fig. 10. Supply/demand gaps given by the MPC strategy with "perfect" or GPR forecasts using a 14-hour sliding window, with respect to the initial gap and the one given by the weekly planning.

First, the paper proposes an alternate model of the problem to bypass the MINLP framework without relaxing the ON/OFF controller constraint of the water tower. Second, a study is carried out of the resilience of the MPC scheme to forecasting errors of PV power generation and grid load, with respect to the sliding window length and to a scheme actual data. Forecasts are updated at each time step, 10 minutes herein. Simulation results show that the use of forecasts degrades the final value of objective function with respect to values obtained when "perfect" forecasts are used. However, the gap between the two cases remains contained and the scheme performs better as the sliding window size gets bigger. The closed-loop structure of the MPC scheme shields it from steep performance degradation due to increasing forecasting error as the forecast horizon gets longer. With increasing sliding window size, the computational cost of the control scheme increases as well, with further cost added by the imperfection of grid load and PV power generation forecasts. In addition, the maximum amplitude of voltage constraint violation, when it occurs, is higher than in the case where data are used.

The next step in this research is to use adjustable time steps for the MPC scheme to alleviate the computational burden. Future developments also include optimal dimensioning of the flexible assets' storage units (biogas storage and volume storage) and adapting the optimisation problem to be robust to forecasting errors by using the forecast confidence intervals provided by the GPR model.

ACKNOWLEDGEMENTS

The authors would like to thank the French Environment and Energy Management Agency (ADEME) for its financial support. They would also like to thank the Smart Occitania consortium, particularly ENEDIS, the French distribution grid operator. This research was partially supported by the supercomputing infrastructure of the NLHPC (ECM-02).

REFERENCES

Bruni, G., Cordiner, S., Mulone, V., Rocco, V., and Spagnolo, F. (2015). A study on the energy management in

domestic micro-grids based on model predictive control strategies. *Energy Conversion and Management*, 102, 50–58.

Dkhili, N., Eynard, J., Thil, S., and Grieu, S. (2020). A survey of modelling and smart management tools for power grids with prolific distributed generation. *Sustainable Energy, Grids and Networks*, 21, 100284.

ENEDIS (2018). Principes d'étude et de développement du réseau pour le raccordement des clients consommateurs et producteurs BT. Technical report.

Gbémou, S., Tolba, H., Thil, S., and Grieu, S. (2019). Global horizontal irradiance forecasting using online sparse gaussian process regression based on quasiperiodic kernels. In *2019 IEEE International Conference on Environment and Electrical Engineering and 2019 IEEE Industrial and Commercial Power Systems Europe (EEEIC/I&CPS Europe)*, 1–6. IEEE.

Haupt, S.E., Copeland, J., Cheng, W.Y.Y., Zhang, Y., Ammann, C., and Sullivan, P. (2016). A method to assess the wind and solar resource and to quantify interannual variability over the United States under current and projected future climate. *Journal of Applied Meteorology and Climatology*, 55(2), 345–363.

Lee, J. and Leyffer, S. (2012). *Mixed integer nonlinear programming*. Springer, New York, NY.

Mohassel, R.R., Fung, A., Mohammadi, F., and Raahemifar, K. (2014). A survey on advanced metering infrastructure. *International Journal of Electrical Power & Energy Systems*, 63, 473–484.

Mori, H. and Ohmi, M. (2005). Probabilistic short-term load forecasting with gaussian processes. In *Proceedings of the 13th International Conference on, Intelligent Systems Application to Power Systems*, 6–pp. IEEE.

Nocedal, J. and Wright, S.J. (2006). *Numerical optimization*. Springer, New York.

Parisio, A., Wiezorek, C., Kyntäjä, T., Elo, J., Strunz, K., and Johansson, K.H. (2017). Cooperative mpc-based energy management for networked microgrids. *IEEE Transactions on Smart Grid*, 8(6), 3066–3074.

Pesaran, M.H.A., Huy, P.D., and Ramachandaramurthy, V.K. (2017). A review of the optimal allocation of distributed generation: Objectives, constraints, methods, and algorithms. *Renewable and Sustainable Energy Reviews*, 75, 293–312.

Petrollese, M., Valverde, L., Cocco, D., Cau, G., and Guerra, J. (2016). Real-time integration of optimal generation scheduling with mpc for the energy management of a renewable hydrogen-based microgrid. *Applied Energy*, 166, 96–106.

Prodan, I. and Zio, E. (2014). A model predictive control framework for reliable microgrid energy management. *International Journal of Electrical Power & Energy Systems*, 61, 399–409.

Rasmussen, C.E. and Williams, C.K.I. (2006). *Gaussian Processes for Machine Learning*. The MIT Press.

Rohani, A., Taki, M., and Abdollahpour, M. (2018). A novel soft computing model (Gaussian process regression with K-fold cross validation) for daily and monthly solar radiation forecasting (Part: I). *Renewable Energy*, 115, 411–422.

Sugihara, H., Yokoyama, K., Saeki, O., Tsuji, K., and Funaki, T. (2013). Economic and efficient voltage management using customer-owned energy storage systems in a distribution network with high penetration of photovoltaic systems. *IEEE Transactions on Power Systems*, 28(1), 102–111.

Sultana, W.R., Sahoo, S.K., Sukchai, S., Yamuna, S., and Venkatesh, D. (2017). A review on state of art development of model predictive control for renewable energy applications. *Renewable and sustainable energy reviews*, 76, 391–406.

Swan, L.G. and Ugursal, V.I. (2009). Modeling of end-use energy consumption in the residential sector: A review of modeling techniques. *Renewable and Sustainable Energy Reviews*, 13(8), 1819–1835.

Tolba, H., Dkhili, N., Nou, J., Eynard, J., Thil, S., and Grieu, S. (2019). GHI forecasting using gaussian process regression: kernel study. *IFAC-PapersOnLine*, 52(4), 455–460.

Wan, C., Zhao, J., Song, Y., Xu, Z., Lin, J., and Hu, Z. (2015). Photovoltaic and solar power forecasting for smart grid energy management. *CSEE Journal of Power and Energy Systems*, 1(4), 38–46.